*J. Fluid Mech.* (1987), *vol.* 185, *pp.* 503–522
*Printed in Great Britain*



# A model for the dynamics of polymers in laminar shear flows

By D. E. KEYES
Department of Mechanical Engineering, Yale University, New Haven, CT 06520, USA

AND F. H. ABERNATHY
Division of Applied Sciences, Harvard University, Cambridge, MA 02138, USA

(Received 5 February 1986 and in revised form 6 January 1987)

A novel primitive model is proposed for the hydrodynamic behaviour of an isolated dissolved polymer molecule in a laminar shear flow. The model, in which inertial effects are neglected, allows for rotation and partial stretching of the molcule, but not for bending. Dilute solutions of flexible long-chain polymers have been experimentally observed to exhibit periodic velocity fluctuations distinct from turbulence over a broad frequency range when flowed in high-shear-rate water-table and pipe configurations. In these experiments, the frequency of the fluctuations does not increase with increasing shear rate; rather, it is lowest in the regions of the flow where the shear is the highest. A manifestation of viscous shear thickening has also been observed in these laminar flows. The proposed polymer representation appears capable of accounting for the salient features of these flows with adjustment of a single dimensionless parameter, a ratio of polymer-spring and solvent-viscosity forces.

## 1. Introduction

Periodic fluctuations in the streamwise component of velocity have been observed in a series of high-shear-rate laminar water-table and pipe flows of dilute (3–18 p.p.m.) solutions of the flexible long-chain polymer polyethylene oxide (PEO). As reported elsewhere (Abernathy *et al.* 1980; Abernathy & He 1984, 1987), these fluctuations disappear if either the polymer concentration or the shear rate is too low, but are reproducibly excited at sufficiently high concentration and shear. The power spectrum of the fluctuations is distinct from that of turbulence, which may be triggered and may coexist at the same flow conditions.

The pronounced structure in the spectrum of the velocity, which the model is advanced to explain, has been observed in two different flow geometries using three different laser-Doppler velocimetry (LDV) techniques. Results from two of these investigations are shown in figures 1 and 2. The spectrum is most narrowly peaked in the LDV measurements in a water-table flow, as shown in figure 1, which is from Abernathy *et al.* (1980). The experimental technique employed selective seeding of the flow with micron-size hydrogen bubbles generated electrolytically upstream of the scattering volume by a wire held spanwise in the flow. The effective scattering volume was the intersection of the plane of the bubbles with the needle-shaped volume defined by the crossed laser beams, which was oriented with its long axis normal to the wall, presenting a small cross-section to the plane of the bubbles.

As the bubble-generating wire was traversed in the direction normal to the wall,

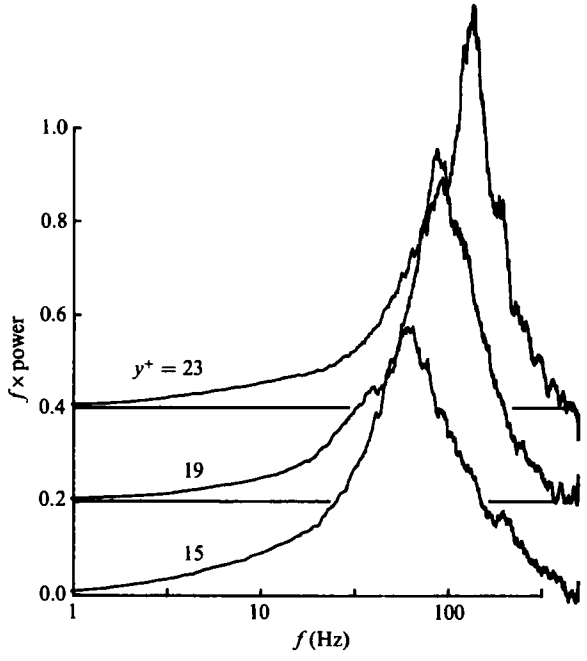


FIGURE 1. Streamwise velocity spectra for a polymer-induced fluctuation water-table flow at three transverse positions in the layer (from Abernathy *et al.* 1980). The axes are frequency times power *vs.* log frequency. For clarity the spectra at $y^+ = 19$ and 23 are offset vertically by 0.2 and 0.4, respectively. The flow parameters are $u_\tau = 3.43$ cm$^2$ s$^{-1}$, $\nu = 0.00905$ cm$^2$ s$^{-1}$, $Re = 1630$. The polymer concentration is 18 p.p.m.

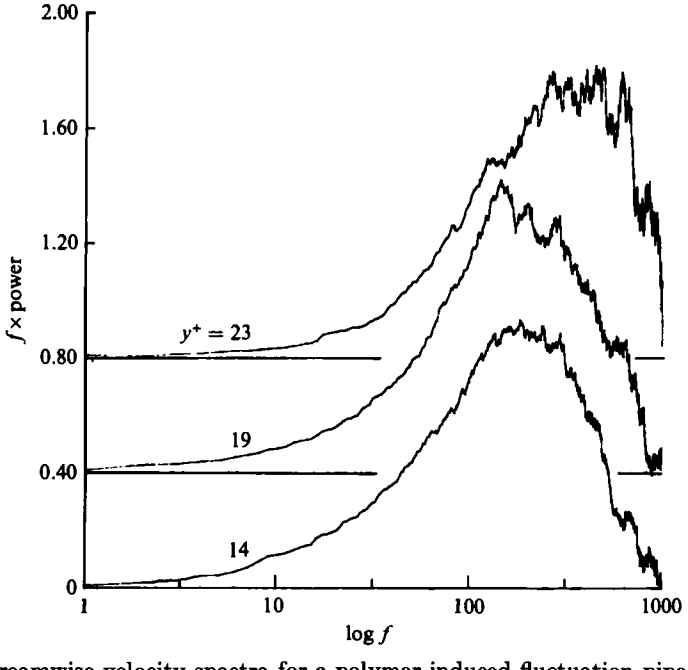


FIGURE 2. Streamwise velocity spectra for a polymer-induced fluctuation pipe flow at three radii (from Abernathy & He 1984). The axes are as in figure 1, with the spectra at $y^+ = 19$ and 23 offset by 0.4 and 0.8, respectively. $Re = 3470$ and the polymer concentration is 10 p.p.m.

the velocity and resulting spectrum was measured at different elevations in the flow. The centre frequency of the peak in the spectrum is lowest near the wall where the shear rate is highest, and higher away from the wall where the shear rate is lower. Further from the wall, at the lowest shear rates, the spectrum (not shown) has no frequency structure. The streamwise velocity spectrum in laminar flows at low shear rates or at low polymer concentrations (or both) is a constant, independent of frequency.

These measurements in two-dimensional water-table flows with a free surface were confirmed in an independent series of measurements in pipe flows, as shown in figure 2, which is from Abernathy & He (1984). In these experiments, a smaller than conventional (0.2 mm × 0.025 mm dia.) laser scattering volume was used with its long axis oriented along the 2.5 mm pipe radius. The flow was uniformly seeded with milk, and the scattering volume was optically traversed in the direction normal to the wall. With the long axis of the scattering volume oriented along the shear-rate gradient the velocity spectra of figure 2 were, as expected, broader than those of figure 1; still, the centre frequency of the peaks increases slightly with distance away from the wall towards the lower shear-rate core of the flow.

The presence of peaks in the spectra of figures 1 and 2 implies coherence of the velocity fluctuations over lengths on the order of centimetres in the flow direction, given the frequencies and the mean flow rates. With the LDV equipment available, it was not possible to construct two-point velocity correlations; however, inferences about correlations in the other directions can be made from available data. The frequency variation normal to the wall explicitly shown in the figures implies little, if any, correlation in this direction. Decreased correlation in the other transverse direction can be inferred from additional water-table experiments using uniform seeding in which the scattering volume was located with its long axis oriented spanwise in the flow. The spectrum of the velocity signal at $y^+ = 14$ was broadly distributed from 30 to 200 Hz, as opposed to the fairly narrow peak about 60 Hz shown at $y^+ = 15$ in figure 1. Such a spectrum is consistent with weak spanwise phase correlation of the velocity signal over the 1.6 mm length of the scattering volume used in these experiments.

Another interesting feature of the dilute-polymer laminar flows is the shear-thickening phenomenon reported in Abernathy & He (1984, 1987). In the pipe flows described therein, the friction factor exhibited a slight increase with increasing Reynolds number, implying an increase of viscosity with shear rate, a feature which cannot be explained with non-deforming polymers.

In a preliminary effort to account for these phenomena, a hybrid ellipsoid-dumbbell polymer model was advanced in Abernathy *et al.* (1980). This fully deterministic model containing a single time constant has been further developed, and shows promise in accounting for three of the most significant features observed in high-strain-rate polymer flows, namely

(i) the dependence of the fluctuation frequency on the local shear rate,

(ii) the dependence of an estimate of the effective viscosity of the mixture on the local shear rate, and

(iii) the local streamwise coherence.

The hybrid model is introduced in §2. Sections 3, 4 and 5 are devoted, respectively, to the three points listed above. We conclude in §6 with a summary and a discussion of the outstanding questions.

## 2. Three rheological bodies

Because of the uncertainty in defining the shape of a macromolecule such as a polymer, protein, or blood cell in solution, and the difficulty of solving the hydrodynamic equations in the domain exterior to such irregular bodies, simple bodies such as ellipsoids, dumbbells, rods and the like have often been employed in rheological contexts to generate intuition and to account qualitatively for the behaviour of the macromolecule–fluid system. In this section, the features of two classical rheological bodies, the rigid ellipsoid and the bead-and-spring dumbbell, are reviewed and combined to obtain a behaviour which resembles that deduced for flexible long-chain polymer coils on the basis of the experimental observations cited above, in a way that no other comparably simple model is likely to be able to do.

### 2.1. *The rigid ellipsoid*

The frequency of the experimentally observed periodic fluctuations in the streamwise velocity component of simple shear flows of dilute polymer solutions in water-table and pipe geometries is suggestive of the frequency of the tumbling of an isolated prolate ellipsoid. As derived in Jeffery (1922), a rigid prolate ellipsoid of revolution with aspect ratio $r$ (defined as $a/b$, where $a$ and $b$ are the semi-major and semi-minor axes, respectively) placed in a low-Reynolds-number shear flow with vorticity $\kappa$, with its long axis in the plane normal to the axis of vorticity, rotates with an angular velocity

$$\dot{\phi} = \kappa \frac{r^2 \cos^2\phi + \sin^2\phi}{r^2+1}, \tag{1}$$

where $\phi$ is the angle between the axis normal to the flow and the major axis of the ellipsoid: see figure 3 for a defining sketch. (A simple shear flow is a superposition of a pure straining motion in a plane, with zero rate of expansion, and a rigid rotation normal to the plane. In the coordinate system shown, the only non-zero components of the strain and rotation tensors are equal to half of the shear rate, and these terms will be used interchangeably herein in describing the magnitude of $\kappa$.) The key assumption made in obtaining (1) consists in setting the net torque on the ellipsoid due to the fluid force to zero. The rotation is rapid in the vicinity of $\phi = 0$, where the ellipsoid is nearly perpendicular to the flow, and slows down in the vicinity of $\phi = \frac{1}{2}\pi$, where the ellipsoid is nearly aligned with the flow. Owing to the symmetry and resulting indistinguishability of the two ends of the ellipsoid, the rotation has a period of just $\pi$. The frequency $f_\pi$ at which flips of $\pi$ rad are executed (the experimentally measurable frequency) is (Jeffery 1922)

$$f_\pi = \frac{\kappa}{\pi(r+1/r)}. \tag{2}$$

This frequency increases linearly with the shear rate, but decreases with increasing aspect ratio. Since the experimental streamwise velocity fluctuation frequency decreases or is nearly stationary with increasing shear rate, the rigid ellipsoid model alone seems incapable of a useful description. However, (2) suggests that a model that is capable of deforming to successively larger aspect ratios with increasing shear rate might prove useful.

### 2.2. *The bead-and-spring dumbbell*

A simple bead-and-spring dumbbell model of a polymer, of the type initially considered in Bird *et al.* (1977) and as sketched in figure 4(*a*), provides a mechanism

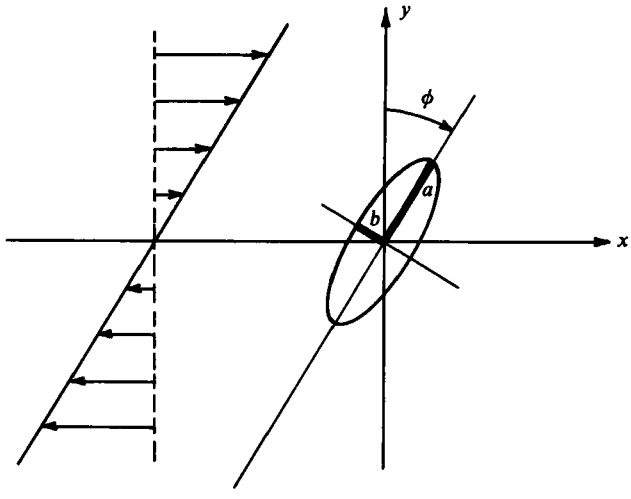


FIGURE 3. Ellipsoid of revolution with aspect ratio $a/b$ rotating in the $(x, y)$-plane of the uniform shear flow $u = \kappa y$, $v = w = 0$.

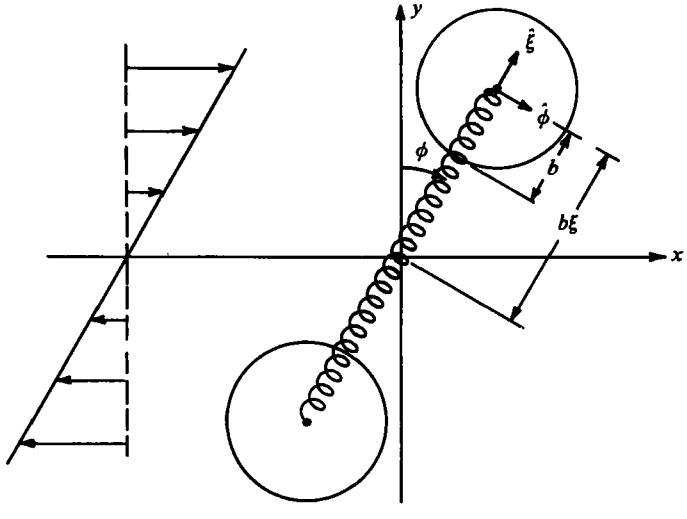


(*a*)

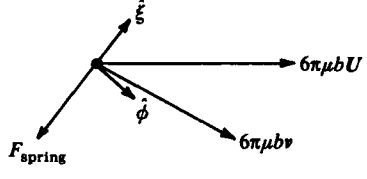


(*b*)

FIGURE 4. (*a*) Bead-and-spring dumbbell rotating and deforming in the $(x, y)$-plane of the uniform shear flow $u = \kappa y$, $v = w = 0$. (*b*) Instantaneous balance of forces on the sphere in the first quadrant.

for deformation. Two spheres of radius $b$ are connected at their centres by a non-bendable spring of semi-elongation $\xi b$, where $\xi$ is a dimensionless length. The spring itself does not interact with the fluid, and the couples on the individual spheres (due to the local shear) are at first ignored, leaving only the net force acting through the centre of each sphere to be taken into account. The sum of the instantaneous drag forces and spring forces on the spheres is set to zero to derive the equations of motion for the body, which is consistent with the non-inertial limit used in deriving (1).

The hydrodynamical force on one of the spheres because of its motion with velocity $\boldsymbol{v}$ relative to that of the fluid $\boldsymbol{U}$, assuming the validity of the Stokes drag formulation and ignoring the presence of the other sphere, is $6\pi\mu b(\boldsymbol{U}-\boldsymbol{v})$. In the local $(\xi,\phi)$-coordinate system, the ambient velocity $\boldsymbol{U}$ at the centre of the sphere is $\hat{\boldsymbol{x}}\kappa b\xi\cos\phi = [\hat{\boldsymbol{\xi}}\kappa b\xi\cos\phi\sin\phi+\hat{\boldsymbol{\phi}}\kappa b\xi\cos^2\phi]$ and the velocity $\boldsymbol{v}$ of the centre of the sphere itself is $[\hat{\boldsymbol{\xi}}b\dot{\xi}+\hat{\boldsymbol{\phi}}b\xi\dot{\phi}]$. In terms of the variables of the bead-and-spring model, the hydrodynamical force becomes

$$\boldsymbol{F}_{\text{fluid}} = 6\pi\mu b[\hat{\boldsymbol{\xi}}(\kappa b\xi\cos\phi\sin\phi - b\dot{\xi})+\hat{\boldsymbol{\phi}}(\kappa b\xi\cos^2\phi - b\xi\dot{\phi})]. \tag{3}$$

Since the counterbalancing spring force is purely radial (see figure 4*b*), the angular component of the fluid force must vanish, yielding

$$\dot{\phi} = \kappa\cos^2\phi. \tag{4}$$

Note that this is the same as the equation governing the rotation of a rigid ellipsoid (1), in the limit as the aspect ratio $r$ of the ellipsoid approaches infinity. However, unlike the rotating finite-aspect-ratio ellipsoid, the dumbbell ultimately becomes aligned with the shear flow and ceases to rotate further.

Let the magnitude of the spring force be written as the product of a Hookean constant $H$ times the displacement of the end of the spring from some non-negative equilibrium extension $\xi_{\text{EQ}}$ so that

$$\boldsymbol{F}_{\text{spring}} = -\hat{\boldsymbol{\xi}}Hb(\xi-\xi_{\text{EQ}}). \tag{5}$$

The sum of the radial forces in (3) and (5) must be zero, yielding the equation for the deformation:

$$\dot{\xi} = \kappa\xi\sin\phi\cos\phi - \frac{H}{6\pi\mu b}(\xi-\xi_{\text{EQ}}). \tag{6}$$

Since the bead-and-spring model described by (4) and (6) does not produce periodic rotations, it alone is unsuitable for modelling the experimentally observed behaviour of the polymers. In other contexts (e.g. chapter 10 of Bird *et al.* 1977), Brownian motion is often invoked to provide a mechanism for tipping the bead-and-spring model out of alignment with the flow, leading to a stochastic model for the behaviour of polymers in a simple shear.

### 2.3. *The hybrid model*

Neither the rigid-ellipsoid nor the dumbbell models alone are capable of explaining the periodic fluctuations that have been observed. However, the combination of (1) and (6) gives a promising model, for present purposes, which possesses both rotational and deformational behaviour. Objections may be raised to the assumption, inherent in (1), that the major axis of the ellipsoid remains in the plane normal to the vortex lines as it tumbles. As speculated by Jeffery and confirmed experimentally by Taylor (1923), a rigid prolate ellipsoid of revolution will precess in its orbits until eventually the minimum-energy configuration is reached in which its major axis is parallel to the vortex lines. However, at small Reynolds numbers the number of

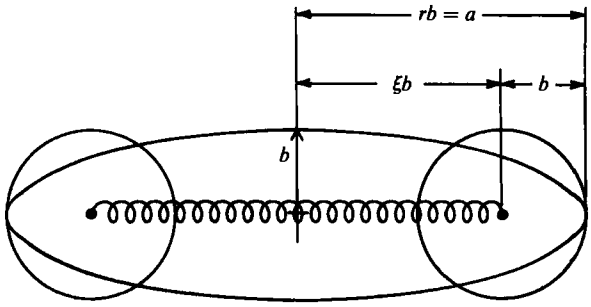


FIGURE 5. The hybrid polymer model, regarded as an ellipsoid for calculating the rotation, and as a bead-and-spring dumbbell for calculating the deformation.

orbits required for the completion of this precession becomes large, a counter-intuitive effect in which increased viscosity leads to slower damping of oscillations. The slight tendency toward alignment with the vortex lines is overbalanced during each flip of the hybrid body by the strong deformational forces tending to pull the ends of the body out in the direction of the flow.

To the end of relating the $r$ of (1) to the $\xi$ of (6), we view the polymer as simultaneously having a dual nature, as sketched in figure 5, where $r = \xi + 1$. The actual effective hydrodynamical shape of the polymer in solution is probably some compromise of the ellipsoid and dumbbell shapes, and is of course considerably less symmetrical than either, in general. However, we shall assume that it is a prolate body of revolution and use whichever of the extreme idealized shapes (ellipsoid or dumbbell) is momentarily convenient. This machination is neither as inconsistent as it may first appear, nor strictly necessary in the kinematical analysis to follow. Bretherton (1962) has shown that almost any physically realizable rigid body of revolution rotates like an equivalent ellipsoid of revolution when placed in a simple shear flow. Thus, such a body obeys (1) for some $r$, provided its axis of symmetry lies initially in the plane normal to the vortex lines. The equivalent aspect ratio $r$ is difficult to compute for general bodies, but has been given for the case of a rigid dumbbell comprised of two equal spheres by Kim & Mifflin (1985).† Their analysis for the interaction of two spheres in low-Reynolds-number flow does not ignore the couples on the individual spheres as we did above. A plot of their numerical results, obtained using the boundary collocation technique and converged to beyond the resolution of the plotter is given in figure 6, along with the line $r = \xi + 1$. It is evident that, within the range of $\xi$ which is of interest (which turns out to be roughly $1 \leqslant \xi < 5$), the inaccuracy entailed by using (1) for the rotation of the polymer, with the slightly underestimated equivalent aspect ratio $r = \xi + 1$, is of small consequence compared with the common idealization, invoked for convenience herein, that polymers may be modelled by some body of revolution to begin with.

At this point, it is desirable to mathematically restate the hybrid polymer model embodied in (1) and (6), slightly generalizing and tidying it. The radial component of the fluid force on each sphere in (3) was computed ignoring the presence of the other. Since the spheres may be quite close (indeed, they may spend part of the cycle less than a diameter apart), we correct for this by multiplying the Stokes drag by a

† The authors are grateful to a reviewer for calling their attention to the work of Kim & Mifflin, which shows that the link between the ellipsoid aspect ratio and the dumbbell sphere separation, which was somewhat arbitrary in the original version, is quantitatively well-founded.

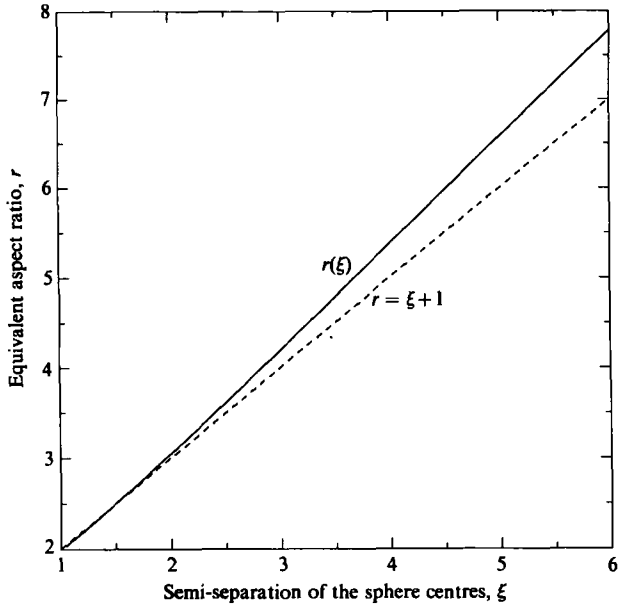


FIGURE 6. Aspect ratio of the equivalent prolate ellipsoid for the rotation of a rigid dumbbell in a simple shear flow (solid curve), and the linear approximation employed herein (dashed curve), as functions of the semi-separation of the sphere centres.

factor $\beta$ which is unity at infinite separation and approaches $\infty$ as the spheres touch, effectively preventing interpenetration. Brenner (1961) has calculated this $\beta$ in the Stokes flow limit, as a function of the dimensionless separation of the centres of the spheres. With $\xi$ as defined above, and with $\alpha = \cosh^{-1}\xi$,

$$\beta = \tfrac{4}{3}\sinh\alpha \sum_{n=1}^{\infty} \frac{n(n+1)}{(2n-1)(2n+3)}\left[\frac{4\cosh^2(n+\frac{1}{2})\alpha + (2n+1)^2\sinh^2\alpha}{2\sinh(2n+1)\alpha - (2n+1)\sinh 2\alpha} - 1\right]. \tag{7}$$

This function is graphed in figure 7. The departure of $\beta(\xi)$ from the simple assumption that $\beta = 1$ is significant within the range of $\xi$ which is of interest, so we incorporate this refinement into the model.

The linear spring law (5) is unlikely to represent a real polymer over wide ranges of deformations. It is desirable to incorporate a softening of the spring at moderate expansions beyond the equilibrium displacement and a hardening of the spring at very large expansions. The softening may be interpreted either as accounting for the reduced number of monomer links in the centre of the polymer holding its extreme ends together when it becomes partially stretched out, or as accounting for an increase in the effective drag on the ends of the polymer due to their relatively greater surface area when they are pulled out, or some combined effect. The hardening is intended to allow for a sharp upper limit on the extension which the polymer can withstand (without breaking). In place of (5) we write, in general

$$\boldsymbol{F}_{\text{spring}} = -\hat{\xi}Hbg(\xi), \tag{8}$$

where a simple choice of the dimensionless $g(\xi)$ is

$$g(\xi) = \frac{\xi - \xi_{\text{EQ}}}{1-(\xi/\xi_{\text{W}})^2}\begin{cases} 1, & \text{if } \xi \leqslant \xi_{\text{EQ}}, \\ (1+\xi-\xi_{\text{EQ}})^{-p}, & \text{if } \xi > \xi_{\text{EQ}}, \end{cases} \tag{9}$$

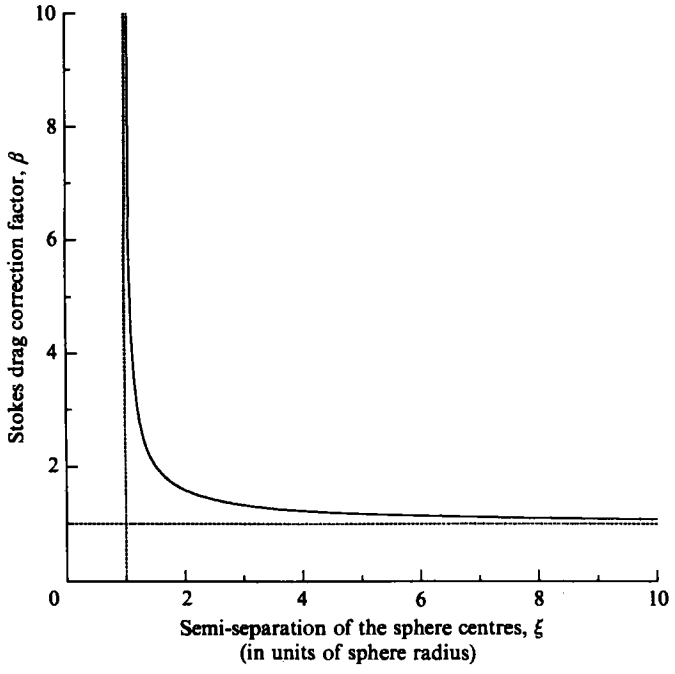


FIGURE 7. The Stokes drag correction factor $\beta$ for the relative motion along the line of centres of two spheres, as a function of the semi-separation of the sphere centres.

where $p > 0$. Apart from the factor in braces, the spring so defined is known as a Fraenkel–Warner spring, and $\xi_W$ is called the Warner constant (Bird *et al.* 1977). The authors have no commitment to the particular form of the spring law in (9). While it possesses the qualitative behaviour described above in an algebraically simple form, it could be replaced by any number of alternatives.

Finally, we non-dimensionalize (1) and (6) by taking $1/\kappa$ as the unit of time. The result is the following coupled set of ordinary differential equations:

$$\begin{pmatrix} \dot{\phi} \\ \dot{\xi} \end{pmatrix} = \begin{pmatrix} [(\xi+1)^2 \cos^2\phi + \sin^2\phi]/[(\xi+1)^2+1] \\ \xi \sin\phi \cos\phi - Cg(\xi)/\beta(\xi) \end{pmatrix}, \tag{10a,b}$$

where $C$, the lone free parameter in the system apart from the functional form of $g$, is the dimensionless number $H/6\pi\mu b\kappa$, a ratio of the spring constant to the viscous drag force on the spheres.

In its undeformed or equilibrium state, the aspect ratio of the prolate ellipsoidal dissolved polymer is assumed to be approximately 3. The approximate equilibrium value of $r_{EQ} = 3$ (or $\xi_{EQ} = 2$) is selected in order to put the fluctuation frequency versus shear rate curve in the experimental region of about 100 Hz for a shear rate of 1000 $s^{-1}$, and is obtained by solving (2) for $r$. When $r_{EQ} = 3$ was first chosen in Abernathy *et al.* (1980), no argument for it was given apart from the magnitude of the observed frequency. Subsequently, the authors have become aware of the extensive literature on the simulation of polymeric structures by means of three-dimensional self-avoiding random walks (e.g. Sŏlc & Stockmayer 1971; Sŏlc 1971; Rubin & Mazur 1975; Rubin, Mazur & Weiss 1976; Rubin & Mazur 1977), which confirms the validity of an aspect ratio of approximately 3 to 1. It should be noted, however, that the equilibrium shapes of such simulations are less symmetrical than

ellipsoids of revolution. Rubin & Mazur (1975) estimate, for instance, that the principal axes of the equivalent ellipsoid for a polymer chain generated as a self-avoiding random walk on a cubic lattice, in the limit of infinitely many links, are in the proportion 3.05:1.77:1.00.

## 3. Periodic limit-cycle behaviour

The hybrid model has been studied quantitatively by numerically integrating the equations of motion (10) with the spring law (9) to their limit cycles over a wide range of $C(= H/6\pi\mu b\kappa)$ from a plausible starting guess $(\phi_0, \xi_0)$. Sample frequency versus shear rate data have been obtained by measuring the period of the orbits asymptotically so obtained. Graphs of $\xi$ versus $\phi$ in the limit cycle for a set of five values for the parameter $C$ are given in figure 8. (Similar curves can be found in figure 9 of Abernathy *et al.* (1980) for the case $p = 0$, and for a wider range of $C$.) All of the results presented herein were obtained with fixed values for the other parameters of $\xi_{EQ} = 2$, $\xi_W = 100$, and $p = 4$. Qualitatively similar behaviour is obtained over neighbouring ranges of the parameters $\xi_{EQ}$ and $\xi_W$. In general, smaller $\xi_{EQ}$ implies higher frequency, with $\xi_{EQ} = 0$ (corresponding to a non-deforming sphere) yielding the highest possible flipping frequency of $\kappa/2\pi$. The motion is not very sensitive to the Warner limit of maximum extension, $\xi_W$, provided that it is set an order of magnitude above the equilibrium extension, as it is here. This is because the polymer does not have time to expand more than a few diameters during any cycle before rotating into regions of the flow (the second and fourth quadrants of figure 4*a*) in which the fluid aids rather than opposes the contractive tendency of the spring.

For large values of $C$, corresponding to low shear rates, the spring length does not change appreciably and the polymer rotates nearly like a rigid ellipsoid, in proportion to the shear rate, as in (1). At intermediate shear rates, the spring expands significantly beyond and contracts to slightly within its equilibrium length during the course of a cycle. The high-aspect-ratio parts of the cycle slow the rotation down, relative to the rigid-body rate based on the equilibrium aspect ratio. For a given $C$ of order unity or smaller, the softening parameter $p$ exerts substantial control over the excursion of $\xi$ in the limit cycle. As $p$ is increased from zero, the polymer can undergo greater and greater expansion at favourable orientations (the first and third quadrants of figure 4*a*). It is the susceptibility to expansion (for sufficiently large $p$) and the concomitant retarding of the rotation (see (10*a*)), that causes the body actually to rotate *less* rapidly as the shear rate is increased over this range. At very high shear rates ($C \ll 1$), the ability of the polymer to deform saturates, and the linear increase of rotation rate with shear rate again prevails. (In the laboratory, breakage of the polymers would probably occur before this saturation effect would be experimentally observable.) Corresponding to the middle curve of figure 8, figure 9 schematically depicts the polymer at its maximum and minimum extensions, superposed simultaneously, for $C = 5.0$.

There is a transition range of $C$, approximately one order of magnitude in width, over which the experimentally observed phenomenon of an absolute decrease in fluctuation frequency $f_\pi$ with increasing shear rate $\kappa$ can be observed. A dimensionless plot of this phenomenon is furnished in figure 10. The Hookean parameter $H$ in $C$ may be fixed so as to centre this range over the centre of the experimentally measurable range of $\kappa$. A dimensional graph of the frequency versus shear-rate behaviour for a particular value of $H/6\pi\mu b$ is given in figure 11. The experimental range of a reduction of 50% in absolute frequency over an increase of 20% in shear

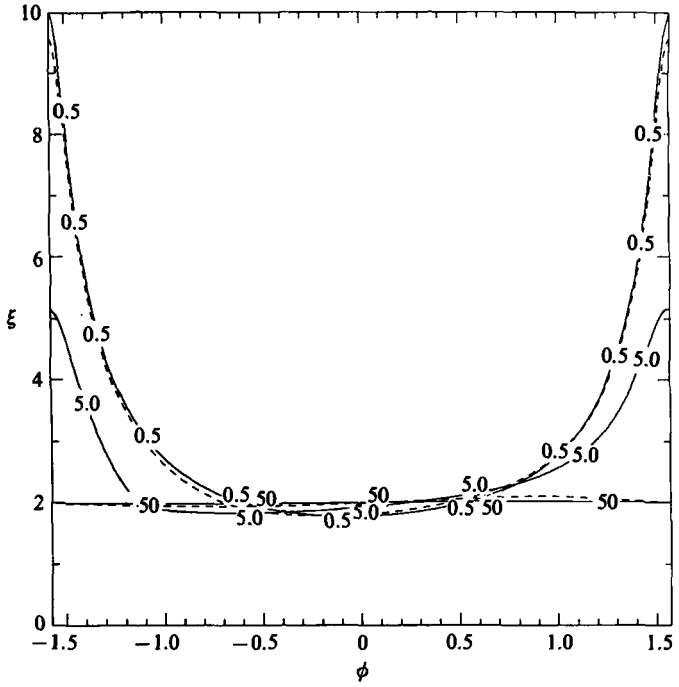


FIGURE 8. Limit-cycle plots of extension $\xi$ as a function of inclination $\phi$ for different values of $C = H/6\pi\mu b\kappa$, spanning the domain of nonlinear frequency versus strain-rate response. The solid curves are labelled with the values $C = 0.5$, 5.0, and 50. The dashed curves near the extreme values are for $C = 1.5$ and 15, and show how the change in the limit cycle with $C$ saturates at both high and low values.

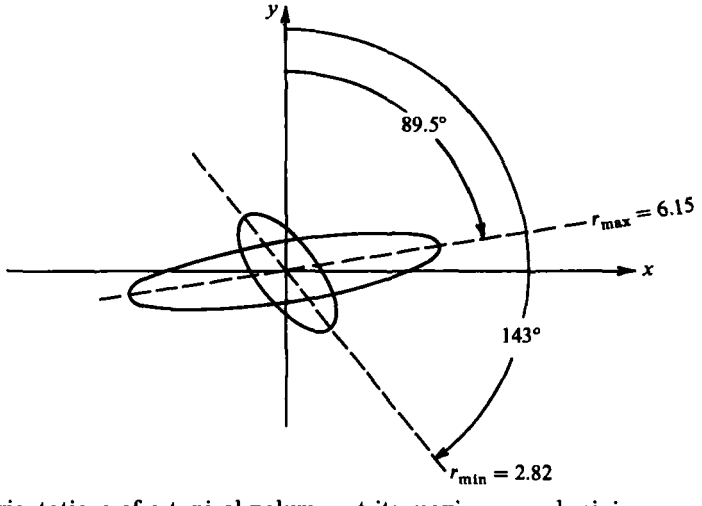


FIGURE 9. Orientations of a typical polymer at its maximum and minimum extensions, superposed, for the case $C = 5.0$.

rate, as displayed in figure 1 is not realized for the particular model and parameters considered above, but it does exhibit a 10% absolute frequency reduction over this range. Considering the crudeness of the model, it does not appear appropriate to attempt to fit precisely a particular set of experiments, such as those presented in figure 1 in which a frequency decrease is evident, or figure 2, in which the frequency

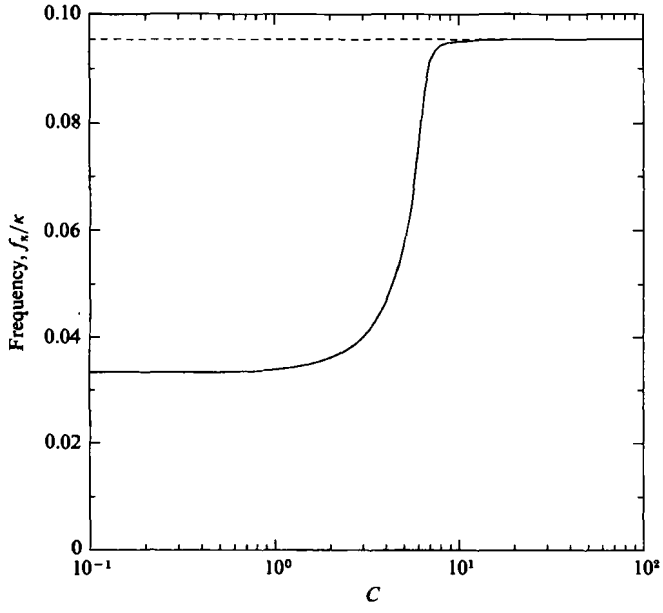


FIGURE 10. Dimensionless frequency versus $C = H/6\pi\mu b\kappa$. The horizontal asymptote at $C \to \infty$ is the rigid-body limit, in which the (dimensional) frequency and strain rate are proportional.

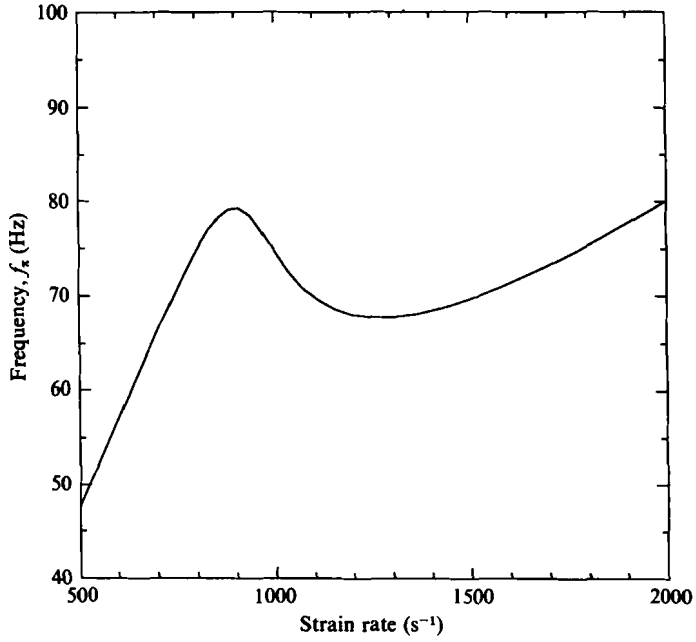


FIGURE 11. Frequency versus strain rate for $H/6\pi\mu b = 6 \times 10^3\ s^{-1}$ in the vicinity of $\kappa = 10^3\ s^{-1}$.

is virtually stationary with increasing shear. However, the softening of the spring and retarding of the rotation provides the potential for creating a range of such behaviour.

Perhaps the greatest of the shortcomings of the present model in its prediction of the polymer flipping frequency is the neglect of the hydrodynamic influence of

nearest neighbours. Coherence of neighbouring polymers in the streamwise direction is presumed (without it, the experimental interpretation of the streamwise velocity fluctuations is invalid), and since such coherence implies constructive interference, it is likely that the effect of nearest neighbours, if it could be properly modelled, would be to boost the predicted fluctuation frequencies at all shear rates, relative to those of the dilute hybrid model.

Another objection to the model might be its infinite resistance to bending. Bending could be modelled by a simple elastic law with a finite spring constant like that proposed for stretching, and the resulting more complicated motion (with another degree of freedom and another parameter) numerically integrated using the two-sphere interaction results of Kim & Mifflin (1985). However, this extra degree of freedom does not seem necessary for the simplest interpretation of the experiments, and there is insufficient experimental information to consider fitting a second parameter. (Indeed, the simple geometry of the two-sphere dumbbell invites several refinements which we have not pursued because the dumbbell is itself merely an idealization from which to obtain the deformational behaviour of a typical polymer in solution.) Bending would undoubtedly be important for polymers attaining much higher aspect ratios, during the parts of their rotations when they are subject to compressive deformational forces.

## 4. Effective viscosity estimate

As discussed in the references, experimental evidence has recently been found for an increase of the effective viscosity of the polymer solution as the shear rate is increased. In figure 8 of Abernathy & He (1984) and a figure forthcoming in Abernathy & He (1987), plots of friction factor versus Reynolds number in pipe flow show that Virk's asymptote for drag-reduced turbulent flow of a dilute polymer solution can also be approached from the *laminar* side as the shear rate is increased past the point where the laminar polymer fluctuations become observable. Such shear-thickening behaviour can also be obtained over a range of shear rates with the hybrid model proposed above from a crude estimate of the limit-cycle-averaged effective viscosity of the suspension.

Deforming ellipsoidal particles in a dilute suspension influence the effective viscosity of the suspension in two ways, which depend on the local shear:

(i) via a rotational motion, in a manner smilar to that of the well-known case of a rigid sphere; and

(ii) via a tensile stretching and contraction, which dissipates energy through hydrodynamical drag.

Since the orbit of the deformable polymer depends on the mean flow in which it is situated, the effective viscosity of a dilute polymer solution is not an intrinsic property of the suspension, but also depends on the mean flow. For the purposes of this section, we consider only the simple shear flow,

$$U = \hat{x}\kappa y, \tag{11}$$

for which we have limit-cycle histories of the polymers from which to work.

The effective viscosity, $\bar{\mu}$, of a dilute suspension in which it is assumed that the particles do not affect the mean flow 'felt' by each other, is customarily defined by the ratio

$$\frac{\bar{\mu}}{\mu^0} = \frac{\bar{E}}{E^0} = 1 + \frac{E^1}{E^0}, \tag{12}$$

where $\mu^0$ is the viscosity of the pure solvent, $\bar{E}$ is the dissipation of the flow integrated over some appropriate reference volume containing a fixed concentration of the suspended particles, and $E^0$ is the reference dissipation of the mean flow integrated over the same volume. The second equation results from defining $E^1 = \bar{E} - E^0$ as the excess dissipation which is due to the rotation and deformation of the particle itself. The integration volume may be defined by the finite walls of some apparatus or by a sphere at large radius, eventually assumed to go to infinity.

For extrapolation to other (dilute) concentrations, (12) is often written in the form

$$\frac{\bar{\mu}}{\mu^0} = 1 + \eta c, \tag{13}$$

where $c$ is the ratio of the volume of the suspended particles $V_p$ in the reference volume to the total reference volume $V^0$ (i.e. the concentration by volume), and $\eta$ is the so-called Einstein coefficient, which is $\frac{5}{2}$ for a suspension of rigid spheres. Note that $\eta$ depends only on the shape, and not on the volume of the suspended particles. Within the range of sizes admissible in the low-Reynolds-number limit, the volume dependence lies only in the factor $c$. In order to allow for the possibility of a time-dependent volume for the deformable suspended polymers, a generalized form of (13) is obtained by writing the instantaneous fractional volume concentration $c$ as the product of the constant equilibrium fractional volume concentration $c_{EQ}$ and the ratio $\gamma$ of the instantaneous polymer volume to the equilibrium polymer volume. On the basis of the ellipsoidal shape of the polymer sketched in figure 5, this ratio might be taken to be linear in the extension coordinate $\xi$:

$$\gamma = \frac{4/3\pi a(\xi)\, b^2}{4/3\pi a_{EQ}\, b^2} = \frac{1+\xi}{1+\xi_{EQ}}.$$

Thus (13) becomes

$$\frac{\bar{\mu}}{\mu^0} = 1 + \gamma\eta c_{EQ}, \tag{14}$$

where the dependencies on the (time-varying) size and shape of the polymers and their (fixed) number density are carried in $\gamma$, $\eta$, and $c_{EQ}$, respectively.

The reference dissipation integrated over $V^0$ is simply

$$E^0 = 2\mu^0 e^0_{ij}\, e^0_{ij}\, V^0, \tag{15}$$

where $2\mu^0 e^0_{ij}$ is the viscous stress tensor of the mean flow. From (12), (14) and (15), we deduce an expression for $\gamma\eta$ for the case of a dilute suspension of deformable polymers with total equilibrium volume $V_p$ in the volume $V^0$:

$$\gamma\eta = \frac{E^1}{2\mu^0 e^0_{ij}\, e^0_{ij}\, V_p}. \tag{16}$$

In analogy with the number-density-independent factor $\eta$ of (13), we refer to composite factor $\gamma\eta$ of (14) as the Einstein coefficient. Since the motion of the polymers is periodic in time $t$, with period $T$, we may define the time averages

$$\langle E^1 \rangle \equiv \frac{1}{T}\int_t^{t+T} E^1(t)\,\mathrm{d}t, \quad \langle \gamma\eta \rangle \equiv \frac{1}{T}\int_t^{t+T} \gamma(t)\,\eta(t)\,\mathrm{d}t.$$

Lacking an exact expression for $E^1(t)$, we approximate it crudely by the sum of separate rotational and deformational terms, $E^1(t) = E^1_{rot}(t) + E^1_{def}(t)$. The rotational term will be instantaneously correct for an ellipsoid at the given aspect ratio and inclination in a uniform shear flow in the absence of deformation, and the

deformational term will be instantaneously correct for the prescribed relative motion of the spheres in a quiescent fluid in the absence of rotation. Thus the spirit in which $E^1$ is approximated is the same as that in which (1) and (6) were combined to form the hybrid polymer model, itself. The approximation has the required property that it reduces to the rigid-ellipsoid results in the low-shear limit in which the polymer undergoes no deformation.

Jeffery (1922) gives an expression for the dissipation rate due to a rigid ellipsoid of aspect ratio $r$ at inclination $\phi$ in its periodic cycle. By regarding $r$ as a known function of time ($r(t) = \xi(t)+1$), where $\xi(t)$ is given along with $\phi(t)$ from the limit-cycle orbits, we may carry this result over to our deforming ellipsoids. To simplify the appearance of Jeffery's formulae, we define an alternative aspect-ratio parameter $\theta(t)$ by $\theta = \cos^{-1}(1/r)$ and four other combinations dependent thereon by:

$$\Theta = \frac{\log[\tan(\frac{1}{2}\theta+\frac{1}{4}\pi)]}{\sin\theta},$$

$$F = \frac{1}{4\sin^4\theta}\left[\frac{2-5\cos^2\theta}{\cos^4\theta+3\Theta}\right],$$

$$G = \frac{1}{\sin^4\theta}\left[2+\frac{1}{\cos^2\theta}-3\Theta\right],$$

and

$$H = \frac{1}{\sin^4\theta}[(2+\cos^2\theta)\Theta-3].$$

Then the dissipation due to the rotation of the polymer is

$$E^1_{\rm rot}(t) = \tfrac{4}{3}\pi ab^2\mu\kappa^2\frac{2}{\cos^2\theta}\left[\left(\frac{1}{H}+\frac{1}{2\cos^2\theta F}\right)\sin^2\phi\cos^2\phi+\frac{1}{(1+\cos^2\theta)G}\cos^2 2\phi\right]. \quad (17)$$

From (11), (16) and (17) we deduce the rotational dissipation coefficient per unit equilibrium volume concentration:

$$[\gamma(t)\eta(t)]_{\rm rot} = \frac{E^1_{\rm rot}(t)}{(2\mu\kappa^2)(\frac{4}{3}\pi a_{\rm EQ}b^2)}$$

$$= \frac{1+\xi}{1+\xi_{\rm EQ}}\frac{1}{\cos^2\theta}\left[\left(\frac{1}{H}+\frac{1}{2\cos^2\theta F}\right)\sin^2\phi\cos^2\phi+\frac{1}{(1+\cos^2\theta)G}\cos^2 2\phi\right]. \quad (18)$$

To estimate the deformational contribution to the dissipation, we first consider the instantaneous dissipation rate due to Stokes–Brenner drag on the sphere at one of the ends of a rotationless dumbbell in a quiescent flow. For a sphere of radius $b$ at the end of the spring, expanding or contracting with an instantaneous velocity $V$ along the axis, the dissipation is $(6\pi b\mu\beta V)V$ with $\beta$ being defined by (7). In terms of the dimensionless semi-extension $\xi$, this component of the velocity is given by $V = \kappa b\dot{\xi}$, and there are two such spheres per polymer, so

$$E^1_{\rm def}(t) = 2\times 6\pi b^3\mu\kappa^2\beta\dot{\xi}^2. \quad (19)$$

Dividing by the same equilibrium ellipsoidal volume used in deriving (18), for consistency with (16), we obtain the deformational dissipation coefficient per unit equilibrium volume concentration:

$$[\gamma(t)\eta(t)]_{\rm def} = \frac{E^1_{\rm def}(t)}{(2\mu\kappa^2)(\frac{4}{3}\pi a_{\rm EQ}b^2)} = \tfrac{9}{2}\beta\frac{\dot{\xi}^2}{(1+\xi_{\rm EQ})}. \quad (20)$$

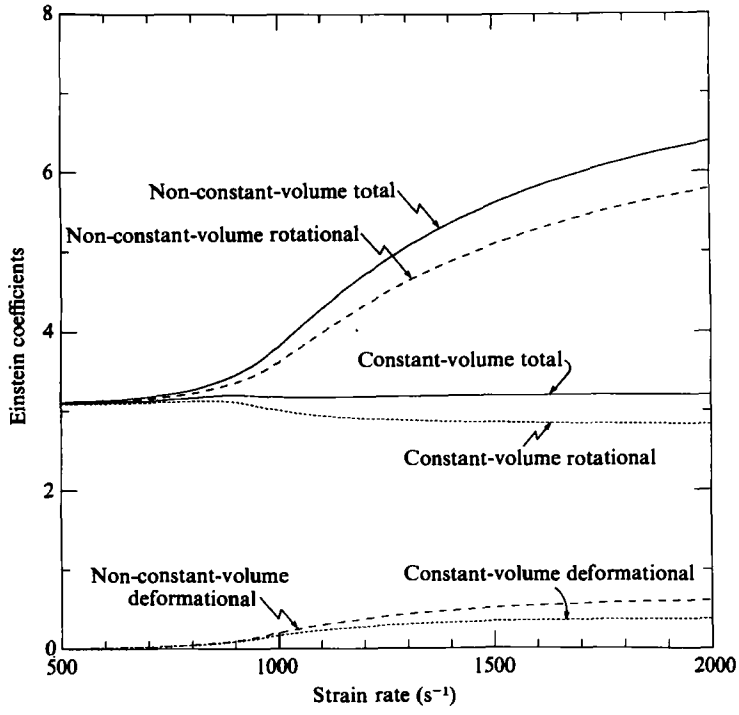


FIGURE 12. The cycle-averaged effective viscosity of a dilute polymer solution under two different assumptions for the volume of the polymer under deformation: non-constant volume (proportional to axial deformation) and constant volume. The Einstein coefficients for the rotational terms alone (equation (18)) are shown in the dashed curves. The solid curves represent the sum of (18) and (20).

Figure 12 contains a graph of the cycle-averaged Einstein coefficient versus shear rate for the polymer whose frequency data was shown in figure 11. The rotational and deformational components are shown separately and their sum is shown in the solid curve. Both components increase with increasing shear rate due to the deformation, which increases the effective volume of the polymer relative to its low-shear undeformed state.

Also plotted in figure 12 is a second set of the same three curves corresponding to the case in which the instantaneous polymer volume is used in the denominators of (18) and (20), rather than the equilibrium volume. This second set of curves corresponds to the rederivation of (18) and (20) with $\gamma = 1$, and would be valid for a polymer which conserves its volume upon deforming to large aspect ratios, in which case (13) may be used in a time-averaged sense without need of the generalization of (14). In the constant-volume case, the cycle-averaged dissipation due to the rotation decreases with increasing shear because a larger fraction of the cycle time is spent nearly aligned with the mean flow, where the ellipsoid presents less of a cross-section to the flow. The total cycle-averaged dissipation does not depart far from the rigid-body value (approximately 3.1 for this polymer) over a large range of strain rates, because the deformation contribution increases accordingly. The behaviour of a real polymer probably lies in between the linear volume-to-aspect ratio behaviour and the volume-conserving behaviour shown here. In any intermediate case, the effective viscosity exhibits a rise in precisely the neighbourhood of shear-rate parameter space where the drop in fluctuation frequency with increasing shear rate is observed.

## 5. A mechanism for local streamwise coherence

Any model which purports to explain the experimentally observed fluctuations should be capable of accounting for the correlation of neighbouring polymers executing their rotations in phase. The correlation should be strong in the streamwise but weak in the spanwise direction and in the other direction normal to the flow in order to account for the experimental findings. The lack of a streamwise correlation mechanism was one of the weak points of the model as presented in Abernathy *et al.* (1980). In that paper, the perturbation velocity field due to the rotational motion of a single ellipsoidal polymer was calculated everywhere in space, after Jeffery (1922). Examination of the perturbation vorticity field showed that it died off rapidly in $r$, and more significantly, was only weakly orientation dependent. This makes hydrodynamic coupling between polymers due to periodic rotational 'kicks' a poor candidate for the correlation mechanism. In contrast, the Brenner–Stokes perturbation flow field due to the expanding and contracting motion of the spheres along their line of centres is strong and strongly orientation-dependent, since these deformations peak at a specific angle. This mechanism (which was not considered in Abernathy *et al.* 1980) periodically sends hydrodynamic signals along rays in the plane of rotation.

The perturbation velocity fields due to the deformational motion of a bead-and-spring dumbbell were calculated after Brenner (1961), and one quadrant of the flow field in an axial plane showing the near and intermediate field is plotted in figure 13($a$, $b$). In the near field, along the axis of deformation, the perturbation velocity falls off like $1/r$ from its maximum at the spherical bead itself. In the far field, the perturbation looks like a dipole and falls off like $1/r^2$. Despite the strength of the deformational signal, there is little opportunity for correlation in the direction normal to the mean flow (the $y$-direction in figure 4$a$). This is apparent from the size of the dimensionless ratio of the distance $\Delta x$ travelled downstream by a polymer convected along at elevation $\Delta y$ relative to the location of a second polymer, during the period that the latter undergoes one elongation–contraction cycle: $\Delta x/\Delta y = (\kappa \Delta y/f_\pi)/\Delta y = \kappa/f_\pi \approx 10$. Polymers separated in $y$ spend very little time in one another's domains of hydrodynamic influence. Only polymers separated streamwise have constant spatial proximity in a direction of strong hydrodynamic signal propagation; hence, only such may be expected to eventually become locked in phase. While we have not made calculations of the interactions of the deformational perturbation flow fields of two or more polymers, we believe that the correlation occurs through this pronounced mechanism. The experimental evidence cited earlier is consistent with the deformational correlation mechanism. At sufficiently low values of $\kappa$, the polymers rotate nearly in proportion to $\kappa$ without much deformation from their equilibrium aspect ratio, as modelled in figure 11. Experimentally, one observes a signal close to white noise, indicating no correlation of these individual polymeric rotations, away from the wall in regions where $\kappa$ is small. Only on the negative-slope side of the frequency maximum of figure 11, where significant deformation occurs, are distinct frequency peaks visible in the sectra. The rotation accounts for the periodicity of the deformational velocity perturbation, but is not a correlation mechanism itself.

As described in Abernathy & He (1984, 1987), the experimental r.m.s. of the perturbation velocity in which the fluctuations are revealed is on the order of the friction velocity $u_\tau$, which is generally 1 cm s$^{-1}$ or a little greater. An estimate of the maximum magnitude of the perturbation velocity due to the deformation of the

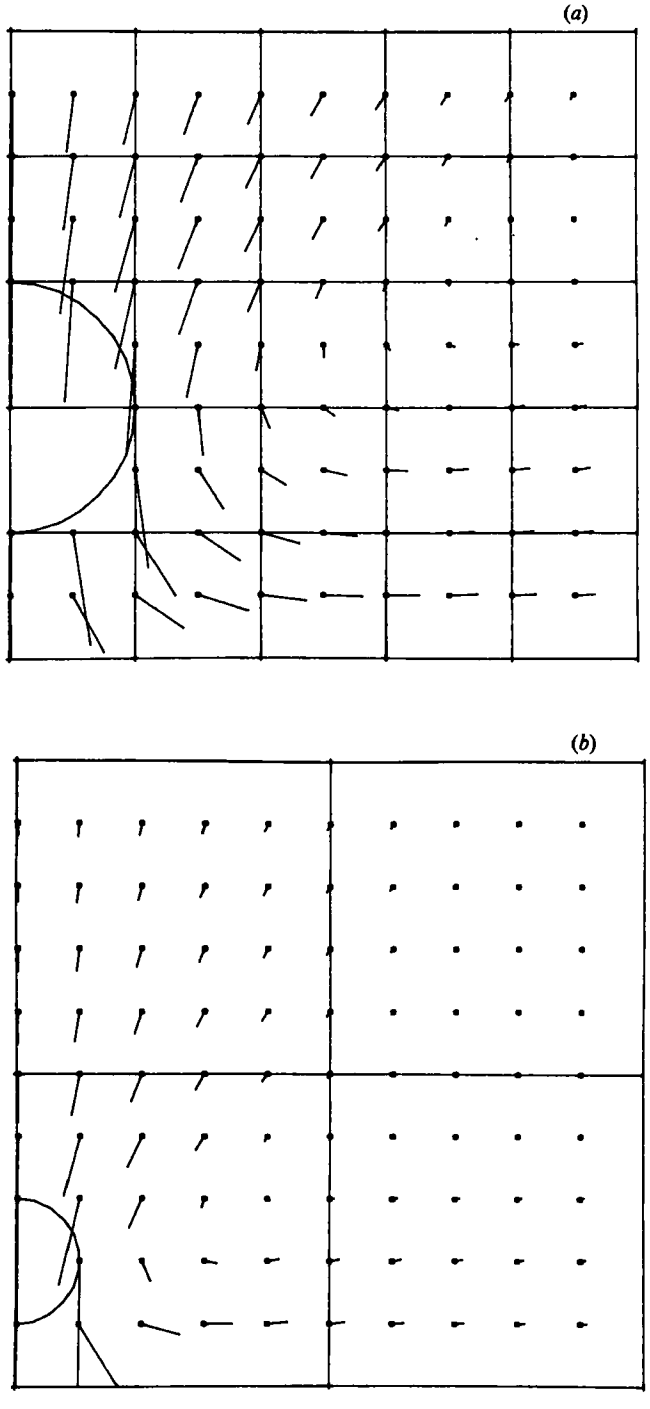


FIGURE 13. (*a*) Velocity streak plot in an axial plane showing the Stokes–Brenner flow due to the relative motion of two spheres along their line of centres in a quiescent fluid. (Only one quadrant is shown.) (*a*) Near field; (*b*) intermediate field.

polymers is furnished by $\max_{t\in[0,T]}\{(\dot{\xi}^2+(\xi\dot{\phi})^2)^{\frac{1}{2}}b\kappa\}$. Note that this is independent of the magnitude of the local velocity, with which the centre of mass of the polymer is advected along, and depends only on the size of the polymer and the local shear rate. In the range of shear rates over which the frequency decreases in figure 11, the maximum dimensionless perturbation velocity $(\dot{\xi}^2+(\xi\dot{\phi})^2)^{\frac{1}{2}}$ over the course of the cycle is fairly constant at a value of about 1.8. With a shear rate $\kappa$ of $10^3\ \mathrm{s}^{-1}$ and a fairly generous typical polymer dimension $b$ of $5\times10^{-5}$ cm, the maximum perturbation velocities that can be expected are approximately $10^{-1}\ \mathrm{cm\ s}^{-1}$. This is at least a factor of 10 too low to account for the experimentally observed energy of the fluctuations. Like the detailed explanation of the coherence of the polymers, the resolution of this disparity in perturbation velocity scales must be left to future investigations that consider the simultaneous interactions of a group of neighbouring polymers. We hypothesize that it is in the superposition of the perturbation fields of many polymers locked in to the same phase that the relatively large r.m.s. perturbation velocities are obtained experimentally.

## 6. Conclusions

A single-parameter family of hybrid ellipsoid–dumbbell models for a polymer in solution has been introduced, and its behaviour in a shear flow has been investigated numerically. The resulting body undergoes periodic rotation and deformation in response to the vorticity and strain of the mean flow. This behaviour is proposed to account for the recently reported periodic fluctuations in the streamwise component of velocity in water-table and pipe flows of dilute polymer solutions, the spectra of which are distinct from turbulence. The hybrid model differs substantially from bead-and-spring dumbbell models previously introduced to explain shear thinning in turbulent shear flows, in that random processes are not invoked.

Through a strain-rate-dependent stretching deformation which causes the polymer aspect ratio to vary by a factor of two or three over the course of one flip, the model is capable of reproducing the observed effect of a decrease of fluctuation frequency with increasing strain rate over a narrow transition region which can be adjusted via a single parameter, a spring constant, to coincide with the experimental range. An estimate of the effective viscosity of the dilute polymer solution has been deduced from the classical Stokes limits for the dissipation due to a rotating ellipsoid and a deforming bead-and-spring dumbbell. This estimate increases with increasing strain rate in the transition range, which is in qualitative agreement with the shear thickening observed in such laminar flows.

Inasmuch as polymer–polymer interactions are not considered, the model cannot account directly for the correlation of the polymer flipping upon which the experimental measurements are based, which is an inherent limitation, and prevents detailed prediction of experimental quantities. However, the Stokes–Brenner axial stretching mechanism shares the same directional properties as the observed correlation, namely strong and intermittent in the streamwise direction and weak in the two normal directions. It is expected that no other mechanism for the correlation of the flipping of neighbouring polymers would be required in a more complete theory.

The authors gratefully acknowledge the support of the National Science Foundation through a grant from the Fluid Mechanics Program (MEA81-21067) and for a pre-doctoral fellowship to the first author. The Division of Applied Sciences of

Harvard University was the generous host during most of this work. The first author also acknowledges the support of the Office of Naval Research (through Contract No. N00014-82-K-0184) and the hospitality of the Yale Research Center for Scientific Computation during manuscript preparation.

## REFERENCES

ABERNATHY, F. H., BERTSCHY, J. R., CHIN, R. W. & KEYES, D. E. 1980 Polymer-induced fluctuations in high-strain rate laminar flows. *J. Rheol.* **24**, 647–665.

ABERNATHY, F. H. & HE, Z.-Y. 1984 Polymer induced velocity fluctuations in dilute drag reducing pipe flows. In *Proc. Third Intl Conf. on Drag Reduction, University of Bristol, UK* (ed. J. H. J. Sellin & R. T. Moses), pp. B.8.1–B.8.8. International Association for Hydraulic Research.

ABERNATHY, F. H. & HE, Z.-Y. 1987 *Friction Factor, Velocity Profile and Spectrum Measurements in Drag Reducing Pipe Flows.* To be submitted to *J. Fluid Mech.*

BIRD, R. B., HASSAGER, O., ARMSTRONG, R. C. & CURTISS, C. F. 1977 *Dynamics of Polymeric Liquids*, vol. 2. Wiley.

BRENNER, H. 1961 The slow motion of a sphere through a viscous fluid towards a plane surface. *Chem. Engng Sci.* **16**, 242–251.

BRETHERTON, F. P. 1962 The motion of rigid particles in a shear flow at low Reynolds number. *J. Fluid Mech.* **14**, 284–304.

JEFFERY, G. B. 1922 The motion of ellipsoidal particles immersed in a viscous fluid. *Proc. R. Soc. Lond.* A **102**, 161–179.

KIM, S. & MIFFLIN, R. T. 1985 The resistance and mobility functions of two equal spheres in low-Reynolds-number flow. *Phys. Fluids*, **28**, 2033–2045.

RUBIN, R. J. & MAZUR, J. 1975 Ordered spans of unrestricted and self-avoiding random-walk models of polymer chains. I. Space-fixed axes. *J. Chem. Phys.* **63**, 5362–5374.

RUBIN, R. J. & MAZUR, J. 1977 Spans of polymer chains measured with respect to chain-fixed axes. *Macromolecules*, **10**, 139–149.

RUBIN, R. J., MAZUR, J. & WEISS, G. H. 1976 Spans of polymer chains. *Pure Appl. Chem.* **46**, 143–148.

SŎLC, K. 1971 Shape of a random-flight chain. *J. Chem. Phys.* **55**, 335–344.

SŎLC, K. & STOCKMAYER, W. H. 1971 Shape of a random-flight chain. *J. Chem. Phys.* **54**, 2756–2757.

TAYLOR, G. I. 1923 The motion of ellipsoidal particles in a viscous fluid. *Proc. R. Soc. Lond.* A **108**, 58–61.